

Regular Article - Living Systems

Collective motility and mechanical waves in cell clusters

Youyuan Deng^{1,2}, Herbert Levine^{1,3}, Xiaoming Mao⁴, and Leonard M. Sander^{4,5,a}

- ¹ Center for Theoretical Biological Physics, Rice University, Houston, TX 77030-1402, USA
- ² Applied Physics Graduate Program, Rice University, Houston, TX 77005-1827, USA
- ³ Department of Physics, Northeastern University, Boston, MA 02115, USA
- ⁴ Department of Physics, University of Michigan, Ann Arbor, MI 48109-1040, USA
- ⁵ Center for the Study of Complex Systems, University of Michigan, Ann Arbor, MI 48109-1107, USA

Received 16 June 2021 / Accepted 11 October 2021 / Published online 15 November 2021 \odot The Author(s), under exclusive licence to EDP Sciences, SIF and Springer-Verlag GmbH Germany, part of Springer Nature 2021

Abstract Epithelial cell clusters often move collectively on a substrate. Mechanical signals play a major role in organizing this behavior. There are a number of experimental observations in these systems which await a comprehensive explanation. These include: the internal strains are tensile even for clusters that expand by proliferation; the tractions on the substrate are often confined to the edges of the cluster; there can exist density waves within the cluster; and for cells in an annulus, there is a transition between expanding clusters with proliferation and the case where cells fill the annulus and rotate around it. We formulate a mechanical model to examine these effects. We use a molecular clutch picture which allows "stalling"—inhibition of cell contraction by external forces. Stalled cells are passive from a physical point of view and the un-stalled cells are active. By attaching cells to the substrate and to each other, and taking into account contact inhibition of locomotion, we get a simple picture for many of these findings as well as predictions that could be tested.

1 Introduction

Eukaryotic cells can often move by a judicious use of forces generated by their cytoskeleton and applied to their surroundings [1]. The observed motion can range from individual cells moving through extracellular space to the coordinated collective motion seen during developmental morphogenetic processes such as gastrulation. In fact, many processes that are important in biology and medicine involve the collective motility of epithelial cell sheets and clusters. In addition to morphogenesis, this type of motion is important during tissue repair, and cancer invasion [2]; for a recent review, see [3]. A particularly striking example occurs as part of the progression of inflammatory breast cancer, where the rapid progress of the disease has been connected to collective cell motion [4,5]. In this paper, we present a simplified mechanical model of the collective motion of cell clusters which is intended to clarify some of the mechanical aspects of these phenomena.

Aside from its biological relevance, collective cell motion is of great interest from the perspective of non-equilibrium physics. Individual cells are active particles [6], able to use their stores of ATP to remain far from equilibrium, do work on their surroundings and on their neighbors, and more generally evade many of the features we associate with non-active materials. Dur-

ing collective motion, these cells coordinate their activity by mechanical coupling, for example by connections such as adherens junctions [7]. This coordination can further be modulated by signaling processes, helping to determine cellular front-back polarity [8] which affects the directionality of applied forces. How the interplay of all these effects gives rise to the observed collective behavior is a challenging conceptual problem. Our model accounts for many of the observed features. For simplicity we focus on a one-dimensional system (lines of cells moving on a substrate). A key feature is a mechanism for cells to transition from being active particles to passive ones, which turns out to underlie a uniform explanation for several distinct experimental results.

Collective motility has been studied in many experiments, for a wide variety of cell types [9]. Major progress has been made by utilizing convenient choices of cells, for example clusters of Madin–Darby Canine Kidney (MDCK) cells, moving on substrates that can be patterned by standard lithography techniques. Our primary interest is the physical forces between the cells. These can be measured by traction force microscopy [10–13]. There is significant evidence from this body of work that the interaction between cells that produces collective behavior is primarily mechanical.

The observed mechanics exhibits some striking features: for example in [10], it was shown that the mechanical stress in the center of a cluster is primarily tensile even though there is cell division and the clus-



^ae-mail: lsander@umich.edu (corresponding author)

ter continually expands in size. In these experiments, tension and cell density varied on the scale of millimeters. Conversely, in [11,12] the inter-cellular tension increased up to a plateau within a few cells of the boundary. In these newer experiments, it was shown that most of the traction on the substrate comes from the outer parts of the cluster; in terms of net force applied, it is as if the center is barely attached to the substrate. This finding is most pronounced at early times, but persists to some extent even as the overall pattern begins to exhibit increasingly random fluctuations. Our model gives a plausible explanation for both these behaviors. We will see that a key parameter is the rate of cell division which adds fluctuations to the cluster interior.

Sometimes, mechanical waves are observed within the cluster [12,14]. In [12], waves originate at the boundary following the release of the confluent layer from confinement. In [14], there is spontaneous generation of repeated waves which the authors attribute to a linear instability of the system. In our model, there are waves that propagate due to the effective finite response rate of the cells when they are released from the passive state by some perturbation. Our model does not show an intrinsic instability as in [14]: we will comment on this below.

In a recent experiment, one-dimensional clusters of cells are observed in annular rings [15]. There is a transition between growth with expansion, when the clusters do not fill the ring, and collective unidirectional motility without cell division, when they do.

There have been a number of theoretical models for the mechanics of these systems, e.g., [11,15–18]. Some authors have modeled the cell cluster as a continuous active medium. In [16], the cluster is treated as a viscous fluid with an effective viscosity and friction coefficient which interacts with a nematic-like polarization field. Continuum models are also used to investigate questions regarding the stability of the advancing tissue boundary [19–21]. A continuum model for wave propagation [17] required feedback between strain and an internal variable of the cell cluster. In [14], a continuum model for waves is given with a coupling between strain and polarity. The model is qualitatively compatible with the experiments for the case of instability waves

In [15], there is a theoretical model for the transition to collective unidirectional motility in an annulus. This treatment considers each cell to be in one of three different states, left polarized, right polarized, or stationary (i.e., passive). Transitions between the states are governed by a master equation which takes into account contact inhibition of locomotion (CIL), i.e., the tendency for cells that collide to move away from each other; see [3] and references therein. This model is very similar to our treatment of the transition, see Sect. 3.3.

There are also models which attempt to fully resolve the shape degrees of freedom of the individual cells, e.g., the cellular Potts models [22], vertex models [23], and phase-field approaches [24,25]. There has been only limited successes in using these models to study the

detailed mechanical state of the cluster and the existence of waves.

Finally, there are simplified cell approaches, ranging from the extreme of treating the cell as a single point [26] to more complex collections of subcellular point-like elements [27]. In [18], cells are treated as composed of two force centers coupled by a contractile spring and which interact with other cells via adhesion forces. The theory includes cell proliferation and CIL. In [11], the cell monolayer as a whole is treated using a molecular clutch scheme [28,29] much like the one we propose below for individual cells. However, the observed, puzzling, feature that the tractions are localized at the edges of the cluster was put in by hand [11]. The focus of [11] is collective durotaxis, which we do not treat here. (An extension of our model to the durotaxis case is in progress).

A more detailed theory of durotaxis using a molecular clutch model was given in [30]. Once more the lack of tractions in the center of the cluster was simply assumed by attaching the cluster to the substrate only at the edges. In our model, below, this feature arises naturally. It may be, of course, that attachments in the center of the cell mass decay because they are not used. However, this does not answer the question of how the lack of tractions arises in the first place. The important point is that our simplified scheme shows how the observed coordination throughout the cluster could be attained by mechanical means alone.

Our model is a simplified cell model in one dimension. We consider cells connected to a substrate by bonds that represent focal adhesions, Cells are joined by bonds and their motion is modulated by CIL. In our version of CIL, cells slow down to avoid hitting any barrier in front. Also, when two cells have a head-to-head collision, one or both of them reverse polarization. (See [18] for a more a more general version of CIL). The polarization affects the distribution of adhesion sites, as is commonly seen in experiment [31]; adhesions are formed in the front and are disassembled in the rear.

The dynamics of each cell involves a cycle of contraction and protrusion, as in many treatments of single-cell motility [32–34]. The contraction is directly coupled to intra- and inter-cellular forces through a linear contraction speed—load relation modeling the effect of many molecular motors [28,29]. If the tensile stress on the cell is too high, it will not be able to contract and will instead "stall." This is analogous to the stationary state in [15]. This notion is compatible with the observation in [11] and in [12] that the interior of the cluster sees small cell speeds/traction and large tension. As we will see below, this notion of stalled cells is key to explaining many of the observed features of cluster mechanics.

Our model is a very simple view of a complex system. Our intention is to isolate the key features that give rise to the surprising effects described above. We differ from earlier schemes by our explicit treatment of the cell motility cycle and the incorporation of the molecular clutch idea. These extra complications have an important payoff: in our model, it is easy to see why we can generate waves and the transition from passive



to active cells is quite natural. Our simple framework explains, within a single scheme, many of the salient mechanical features of this class of systems.

2 One-dimensional model

In this section, we describe our model for collective motility.

2.1 Cell motility and the molecular clutch model

Our starting point is the assumption of a motility cycle: cells first contract and partially detach from the substrate by breaking adhesive bonds (more in the back than in the front), and then the cell protrudes forward. Bonds can re-attach after detaching and after cell protrusion. The cell then contracts again.

In [18,35], each cell is considered to be composed of two subcellular elements that interact with a fixed active contractile spring force. Some previous work [33,34] assumed that the cells have a fixed contraction speed. Both of these assumptions are rather simplified views of the complex process of myosin motor mini-filaments walking along actin fibers. Here, we use the model of [28,29]. In this more realistic account, the molecular motors that drive contraction have a nontrivial force-velocity curve and thereby allow the cell to pause contraction when the tension applied is too large. The advantage of this point of view, as we have mentioned above, is that it gives a natural account of cell stalling.

We picture the cell as a one-dimensional "bar" which is uniformly compressed around its midpoint by the contracting actin cytoskeleton (Fig. 1). We assume the myosin motors to be concentrated at the midpoint dividing the cell into front/back halves of equal lengths L(t). The retarding force acting against contraction is generated by the adhesions to the substrate and the connections to the other cells. This force is the same as the tension, T, at the cell midpoint, since the cell is in force balance. The condition for stalling is that T is greater than T_s , the stall tension. We denote the force felt by each cell's head as F_h . This force will play a role in our formulation of contact inhibition of locomotion (CIL), see Sect. 2.2.

In a time step of length dt, the half-length contracts from L to L - dL, where

$$dL = dt f(T)g(F_h). (1)$$

The speed-load curve of the molecular clutch [28] is:

$$f(T) = \begin{cases} v_f & \text{if } T \le 0 \\ v_f (1 - T/T_s) & \text{if } 0 < T < T_s \\ 0 & \text{if } T \ge T_s. \end{cases}$$
 (2)

The factor $q(F_h)$ is related to CIL. For a freely moving cell, $g(F_h) = 1$. The full definition will be given in Sect. 2.2.

The cell starts each contraction cycle with half-length L_0 . It then contracts for multiple steps according to Eq. 1, before reaching the minimum half-length of $(1 - r_{contr})L_0$. Afterward, it reverts to L_0 by protruding forward quickly and then enters the next contraction cycle. The protrusion part of the cycle is intended to represent the extension of the forward part of the cell which is not connected to the substrate, and its subsequent attachment. Since this step does not, in the model and in reality, require detachment of adhesions, it is reasonable to assume that it has a short time scale.

The cell is attached to substrate (assumed to be rigid) with adhesion bonds, which describe trans-membrane proteins such as integrin. We represent these as a number of springs with rest length zero and spring constant k. Consider a cell whose midpoint has coordinate x_c . At the beginning of a contraction cycle, a series of springs is formed with one end on cell body at $x_i^{(c)}$ and the other on substrate at $x_i^{(s)} = x_i^{(c)}$. The index i runs over the front and back set of adhesions. All adhesions are randomly positioned according to truncated Gaussian probability distributions, except that two adhesions are always placed at the ends.

Formally, adhesion indices run over $i = -N_{adh,back}$, $-N_{adh,back}+1,\ldots,-1,1,2,\ldots,N_{adh,front},$ where negative i indicates an adhesion in the back half, and positive the front. In this process, two adhesions of indices $i = N_{adh,front}, -N_{adh,back}$ form at front/back end of the cell, respectively, and the others are placed by drawing the relative positions randomly:

$$r_i^{(c)} = \frac{x_i^{(c)} - x_c}{x_{N_{adh,front}}^{(c)} - x_c}$$

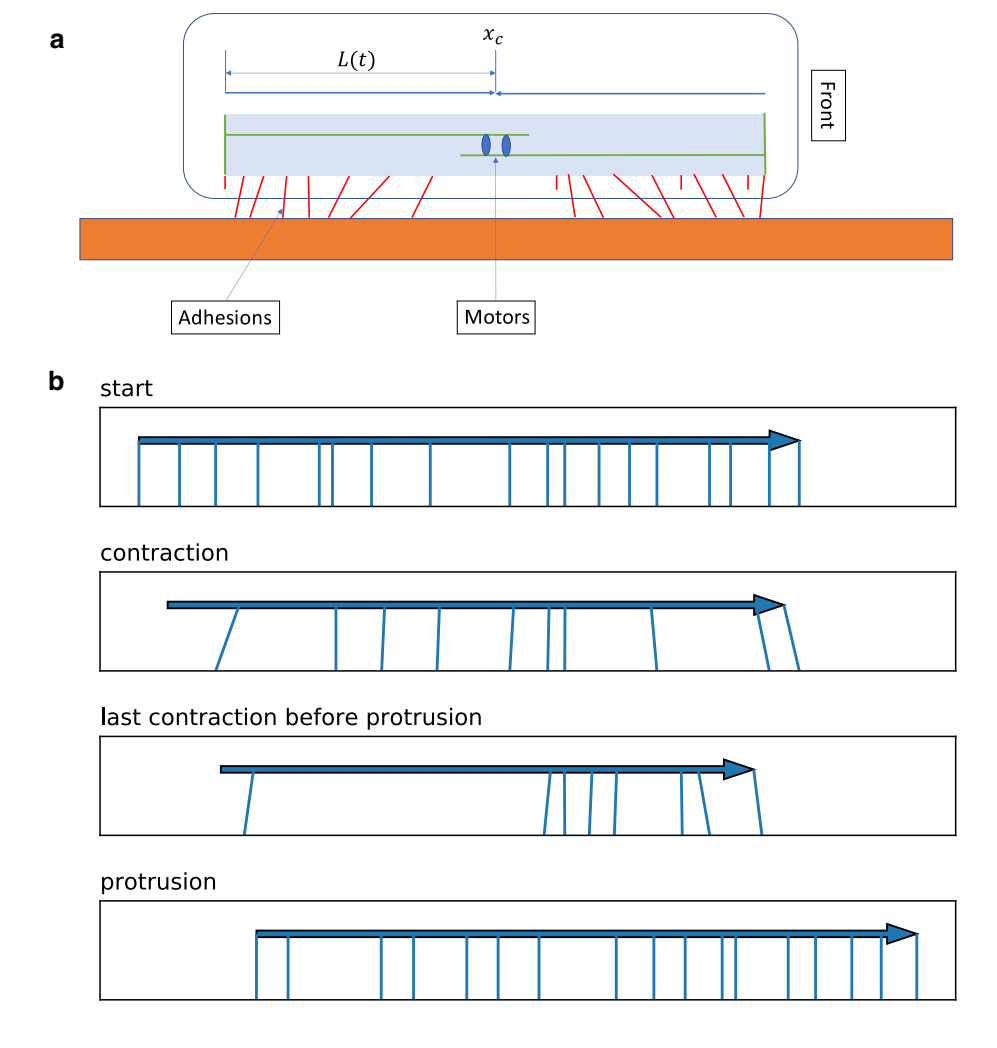
$$\approx \begin{cases}
= -1 & \text{if } i = -N_{adh,back} \\
= 1 & \text{if } i = N_{adh,front} \\
\overline{\mathcal{N}}(\mu = \frac{i}{N_{adh,back}}, \\
\sigma = \frac{1}{4N_{adh,back}}) & \text{if } i = -N_{adh,back} + 1, \dots, -1 \\
\overline{\mathcal{N}}(\mu = \frac{i}{N_{adh,front}}, \\
\sigma = \frac{1}{4N_{adh,front}}) & \text{if } i = 1, \dots, N_{adh,front} - 1.
\end{cases}$$

 $\overline{\mathcal{N}}$ denotes the normal distribution truncated to within [-1,1], so as to always lie within the cell body. We define the front/back polarity by assigning $N_{adh,front} > N_{adh,back}$, i.e., the front half has more adhesions (see Table 1). This is a simplification of the polarized distribution described earlier in [33].

As the cell body contracts, the $x_i^{(c)}$ change, but the absolute coordinates $x_i^{(s)}$ are unchanged under a rigid substrate assumption. Therefore, the *i*-th adhesion is stretched because $x_i^{(c)} \neq x_i^{(s)}$, and exerts a force $f_i =$ $k(x_i^{(s)}-x_i^{(c)})$ on the cell. The adhesions can detach when f_i becomes large. We take the rate of detachment to be governed by Bell's Law:



Fig. 1 a One-dimensional model for a single cell. The red lines are springs with spring constant k, representing adhesions to substrate. The adhesions detach with rate k_{off} and attach with rate $k_{\rm on}$. The cell length contracts according to Eq. 1. At the start of a contraction cycle, more adhesions form in the front half than in back. In the figure, the long bonds represent adhesions that attached to the substrate and the shorter ones represent ones that have detached. The heights of cellular components are for illustration only—the model is one dimensional. **b** Snapshots of key steps during contraction cycles



$$k_{\text{off}} = K \exp(f_i/F_d),\tag{4}$$

where F_d is the critical detachment force. The adhesions revert to zero length when detached. Afterward, they randomly reattach with a constant rate K.

Elastic relaxation is a much faster process than any biochemical process. This is because the elastic elements of a cell cluster relax with a rate connected to the speed of sound. Even in a viscous disordered medium such as a cell with its cytoskeleton and concomitant adhesion proteins, this is surely much faster than the contraction and division processes, which occur on the scale of minutes.

In our model, cells undergo immediate mechanical equilibration of the springs by shifting midpoint positions x_c after each biochemical change, i.e., each contraction and any detachment/attachment of adhesions. Since each half of the cell body is in equilibrium, the tension T in Eq. 1 must be equal to the total force exerted on the half-body by the adhesions, f_i , and with adjacent cells, f_{inter} :

$$T = \sum_{\text{half cell}} (f_i + f_{inter}) \tag{5}$$

The cell contracts by a maximum ratio r_{contr} . Then, it "protrudes" by reverting L(t) to L_0 and placing the back end at the $x_i^{(c)}$ of the current rear-most adhesion, as in the models of [33,34]. In a cluster of multiple cells, each cell is only allowed to protrude to occupy the intercellular space, and is prevented from overlapping with the neighboring cell, so they may protrude to a length smaller than L_0 .

Our picture of a single cell means that it will translate uniformly in the forward direction, that is, the direction where there are more adhesive bonds. We neglect random reversals of polarization. We believe that random reversals must be a minor effect in the experiments we treat since the cell clusters do organize to spread, as in [10] and to coherently rotate around an annulus as in [15]. Therefore, we only focus on reversals induced by CIL, as in the next section.

2.2 Contact inhibition of locomotion

Suppose the cell runs into a barrier (such as another cell) in front that applies a force F_h on the cell. Then, we modify the contraction (recall Eq. 1):



Table 1 Parameters in one-dimensional model

Symbol	Meaning	Value
L_0	Cell's (maximum) half-length at the beginning of each contraction cycle	$5~\mu$ m
v_f	Cell's free(maximum) contraction speed, w.r.t half-length	$3 \mu m/h$
$r_{ m contr}$	Cell's maximum allowed contraction ratio	20%
T_s	Cell's stall tension	10 nN
F_{hs}	Cell's head-stopping force	1.5 nN
l_0	Rest length of inter-cellular adhesions, also the initial inter-cellular separation except for the pre-confinement modeling	$5~\mu m$
k	Spring constant of cell-cell and cell-substrate adhesions	$1 \text{ nN} / \mu \text{ m}$
K	Reattachment rate and coefficient in detachment rate expression of cell-substrate adhesion	6/h
F_d	Critical force for detachment of cell–substrate adhesions	$0.75 \mathrm{~nN}$
$T_{ m div}$	Threshold tension of cell division	$0.99 \ T_s$
$k_{ m div}$	Rate of cell division once $T \geq T_{\rm div}$	0.6/h
$N_{\rm adh,back}$	Number of adhesions to substrate in back half	8
$N_{\rm adh,front}$	Number of adhesions to substrate in front half	10
$\mathrm{d}t$	Time step size	1 min

$$g(F_h) = \begin{cases} 1 & \text{if } F_h \ge 0\\ (1 + F_h/F_{hs}) & \text{if } -F_{hs} < F_h < 0\\ 0 & \text{if } T \le -F_{hs}. \end{cases}$$
 (6)

where F_h takes positive sign when aligned with cell back-to-front vector. Thus, when the cell in front pulls on the cell in question, $F_h > 0$ and there is no suppression of motility. In this work, cases where $F_h < 0$ are always transient as expanding cell clusters are primarily tensile. Thus, cells 'run into each other' only in the initial, confined state. F_{hs} is the scale of the force required to stop the cell. The rationale of Eq. 6 is that cells may actively slow down their motility to mitigate collisions.

In addition to the slow-down, cells can actively alter their direction of movement to avoid collision. In one dimension, there are two possible polarities, left or right. We have defined the polarity by the distribution of adhesions—the half with more adhesions is the front half; cells always protrude toward the front. For a cell that is in front-to-front collision against another, contact inhibition results in disassembly and assembly of adhesion complexes in front and back, respectively. We represent this process by randomly relocating detached cell-substrate adhesions in the front half to the back with rate:

$$k_r = K \exp(F_h/F_{hs}), \tag{7}$$

excluding the one located at the front end. The details of the placement of the relocated adhesions are described in the supplement (Sect. 1).

Once the current rear half has more cell–substrate adhesions, the cell flips polarity, i.e., it protrudes from the end which now has more adhesions. For simplicity, we take the same prefactor as in Eq. (4).

2.3 Formation of a cluster

To form a cluster, the nearest ends of adjacent cells are joined by a spring with constant k, and nonzero rest length l_0 . (For simplicity, we use the same k for the cellcell junctions and the cell-substrate adhesions.) This elastic bond represents not only the adherens junctions between cells, but also the elasticity of the cell body. For example, it is known that when cells on a surface are stretched, they flatten by elastically deforming. The spring is intended to incorporate both effects.

A modification is necessary for the inter-cellular springs. For an isotropic harmonic spring with rest length l_0 , the potential energy is $V(\mathbf{x_1}, \mathbf{x_2}) \propto (|\mathbf{x_1} - \mathbf{x_2}|)$ $|\mathbf{x_2}| - l_0)^2$. To account for volume exclusion, the intercellular adhesion should not allow an equilibrium where two connected cells intrude into each other. Thus, we take $V(\mathbf{x_1}, \mathbf{x_2}) \propto |\mathbf{x_1} - \mathbf{x_2} - \mathbf{l_0}|^2$, with $\mathbf{l_0}$ being a vector.

In Sect. S2 of the supplement, we demonstrate the scheme for two interacting cells.

2.4 Cell division

In [18,35], the idea is introduced that cells are likely to divide if the intra-cellular tension is large enough. It has long been discussed that spatial constraints control cell division [36–38]. Here, we take the point of view that cells start out so confined that their division rate is negligible. Thus, only in the unconfined state, when the cells are under tension will we have significant proliferation.

To implement this, at each step, if a cell's tension Tis greater than $T_{\rm div}$, a critical tension, it divides with constant probability $dt r_{\text{div}}$. Upon division, a newborn cell of the same polarity is inserted next to the current cell, randomly on the left or right. The new cell virtually protrudes in place to avoid overlapping (see the discussion in Sect. 2.1). The nearest ends from adjacent cells



are then connected. When the new cell is introduced, the system is no longer in mechanical equilibrium. We therefore equilibrate after this step.

2.5 Algorithm

The following is our complete algorithm:

- Start each cell with length $2L_0$. Initialize all the adhesions to be at their rest length.
- For each time step dt,
 - 1. For each cell, compute T according to Eq. 5; contract according to Eq. 1; if the cell has reached $r_{\rm contr}$, protrude; in cases when no adhesions remain attached to substrate, wait for next step. Adhesions are stretched. Equilibrate the cell cluster by shifting $\{x_c\}$.
 - 2. For each cell, test for detachment of cell–substrate adhesions using Eq. 4, i.e., detach with probability $k_{\rm off} dt$. Equilibrate.
 - 3. For each cell, attach the free adhesions with probability Kdt. Equilibrate.
 - 4. For each cell, apply contact inhibition of locomotion (CIL). Equilibrate.
 - 5. For each cell, test for cell division, i.e., divide with probability $dt r_{\text{div}}$ if $T \geq T_{\text{div}}$. Equilibrate.

Figure 1b illustrates several of the key steps.

2.6 Parameters

Model parameters are listed in Table 1. We chose the parameters to be representative of cells like MDCK, but this model is certainly not intended to fit a particular experiment. Of course, parameters like L_0 , the cell size and l_0 , the adhesion rest length, are simply typical cell parameters. The time step, dt, is a simulation parameter

To choose v_f , we note that it is of the order of the free cell speed. For MDCK, this is around 3μ m/h [39, 40]. Note that v_f is consistent with the value in [30] Table 1.

For the stall force, our numbers are of the same order as those in [29] (Table S1). The parameter F_d should be thought of as representing the detachment of hundreds of bonds—real cells do not have 18 adhesions as our model cells do. For the same reason, K, k, and F_d should be regarded as effective parameters associated with an entire focal adhesion. They give reasonable results for the entire complex, as we will see.

Our qualitative results depend very weakly on the exact numbers we use. For example, F_{hs} , the headstopping force (steric hindrance) could be larger without changing the results qualitatively. Our values for $T_{\rm div}$ and $k_{\rm div}$ are consistent with the data on waves.

3 Simulation results

3.1 Cluster dynamics without cell division

Previous models for the motility cycle [33,34] are the limit of $T_s \to \infty$ of our current approach. For a free cell, this makes little difference so our results are similar. (For an animation of a single free-moving cell, see SI Movie S1.)

For collective effects, we started by simulating two cells, aligned head-to-head. As the simulation starts, the two cells begin to collide. Because of CIL, at least one of the two cells will eventually change its polarity. When one cell flips, the two cells will move together as a translating cluster. Due to the finite time step size, both cells may flip at the same step, leading to a static situation. See SI Section 2 and SI Movies S2 and S3 for more details. We will see that these two basic choices, a static cluster with an equilibrated tug-of-war versus a translating state, also characterize multicellular clusters.

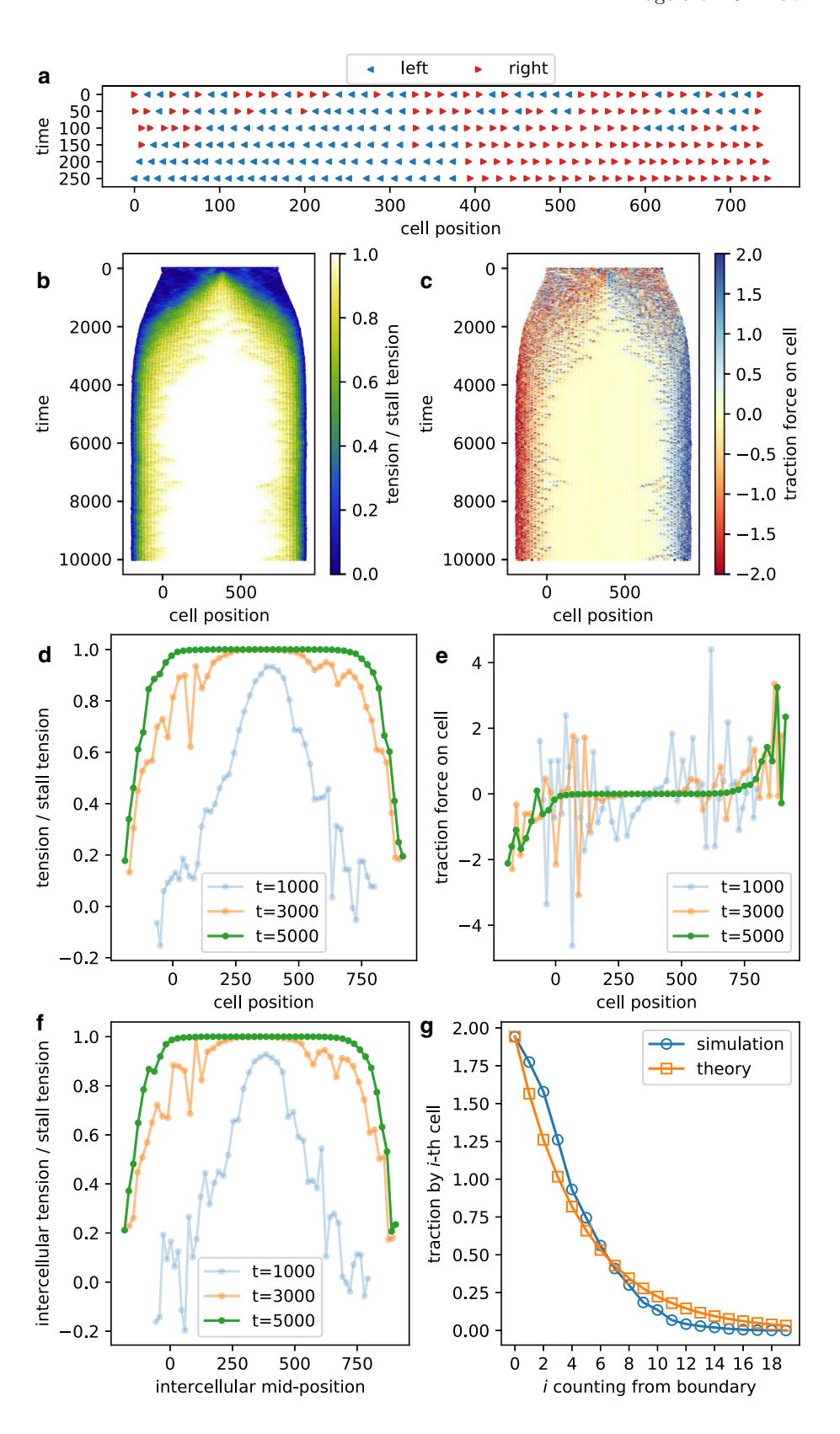
For 50 cells connected by springs with random initial polarity, we used the dynamics described in Sect. 2. In Fig. 2, we show results from one simulation for the polarity, cell tension, force between cell and substrate, and inter-cellular tension. Note that after initial transients the colony settles down with large domains of like polarity (Fig. 2a, SI Fig. 5a) pulling on each other. This is one of two possible outcomes; the other is that the large majority of cells move in one direction and the whole cluster translates.

For our initial conditions with random polarity for 50 cells, both outcomes occur with roughly equal likelihood. In SI Sect. 3 we show that the tug-of-war state is increasingly likely as the number of cells increases. The presence of an initial confinement period, as in most of the experimental protocols, also probably biases the outcome in favor of expansion rather than translation. We will discuss that initial condition later. Here, we consider simulations that lead to tissue expansion with the majority of the cells on the left moving left and those on the right to the right. In the case shown in the figure, we have domains of similar size.

There are interesting features in Fig. 2 that closely correspond to experimental observations. Once the expansion slows, the traction force becomes confined to the edges of the colony, even though all of the cells are attached to the substrate (Fig. 2c, e). This is because the interior cells are mostly stalled (not contracting) and the forces on either end of each domain balance (Fig. 2b, d). Only at the edges are the cells pulling outward. These traction forces at the edges eventually transmit stress to the interior via cell-cell junctions, which are therefore under large tension which can approach T_s , the stall tension (Fig. 2f, SI Fig. 5d). Thus, interior cells are attached, but are not generating traction, see Eqs. (1,2,5). The tension originates from non-stalled active edge cells. Also note that the intercellular springs are tensile except for early transients [11, 12].



Fig. 2 A simulated cell cluster without proliferation. a Polarity of the cells at select time steps during initial transient. They eventually form two similar-sized domains. b Kymograph of tension at each cell's midpoint. Note the stalling of the interior. \mathbf{c} Kymograph of traction force on each cell by substrate. The kymographs shown here are composed of discrete points in space-time coordinate systems where each point represents a cell or an inter-cellular spring at a specific time step. d, e Same quantities as **b**, **c**, at select time steps. Note how the interior cells gradually become stalled. fInter-cellular force at select time steps, the main source of stalling tension in the interior. g Average traction on the left-most cells during the latter half of the trajectory, and predicted values from the simple theory discussed in the text





Traction force fluctuates, so we averaged the traction by each cell over the latter half of the trajectory; see Fig. 2g. One can read off from Fig. 2d–g that intra- and inter-cellular tension accumulates from the outermost cells inward, while the traction exerted by each cell monotonically approaches zero. We have shown that the accumulation leads to stalling of the interior, but why is such monotonic behavior seen within the active edge layers?

It is sensible to assume that each cell's net traction is made possible by protrusion, without which the forces from different cell–substrate bonds of the same cell cancel each other. Since the protrusion algorithm prevents overlapping, one might be tempted attribute this to the fact that inner cells tend to protrude less than outer cells. This however gives the wrong result because intercellular space increases inward with inter-cellular force.

A plausible explanation lies in the speed–load curve. Roughly speaking, more frequent protrusion, i.e., shorter contraction cycle, leads to larger average traction. Thus, the mean value $\langle F_{trac} \rangle \propto 1/T_{cycle} \propto \langle \text{contraction speed} \rangle \propto \langle f(T) \rangle$. We index the cells with i starting from 0 on the outside. Then, we further approximate $T(i\text{-th cell}) = \sum_{i' < i} F_{trac}(i'\text{-th cell})$, and calibrate the proportionality coefficient using the 0-th cell (i.e., setting $\langle F_{trac} \rangle$ to the simulation value), we obtain the "theory" curve in Fig. 2g, which is comparable to the observed simulation values.

Given the curve in Fig. 2g, it is clear that a minimum number of active edge cells are needed to accumulate stress to reach stalling. On the other hand, stalled, non-contracting cells are effectively passive. Their adhesions to the substrate still randomly detach/reattach, amounting to an effective viscous friction. The friction is similar for active cells, but it is the only cellsubstrate interaction for stalled cells. Of course, the viscous friction force is zero unless the cells actually move. It is therefore natural to speculate that the polarity of stalled cells is irrelevant, so we can have force-balanced non-translating clusters, with unequalsized polarity domains, so long as each domain contains more than the required minimum number of edge cells. Fig. 3a-c and SI Fig. 6 show an example of this type of behavior.

On the other hand, when the left or right domain has too few cells, the accumulated tension is not enough and the interior cells are not stalled, but they still have uniformly weaker contraction compared to edge cells (Fig. 3d-f, SI Fig. 7). In this case, the whole colony translates in bulk. The limiting case is when all cells end up having the same polarity (see SI Figs. 8, 9). As discussed above, starting from a completely randomized polarity state both types of solution emerge dynamically.

The localization of traction and motility shown in Figs. 2 and 3 qualitatively agrees with experimental findings [11,12]. This agreement relies on the fact that cells in the center are effectively stalled by tensile stress. Note however, that as a function of time in our simulation, the width of the cell colony saturates due to the equilibrium between the traction forces at edges

and the interior forces on individual cells; on the other hand, those experiments observed continued expansion for ~ 10 h. This is, in our view, connected to the increasing importance of cell division, which occurs more frequently when cells are subject to mechanical stretching [36–38]. We will consider this effect below. The "head-stopping" aspect of CIL can lead to similar localization for confined clusters, as we will see.

3.2 Pre-confinement, mechanical waves, and cell division

A common experimental procedure for studying tissue expansion is that cells are first confined within a rectangular stencil before that barrier is removed and cells are allowed to expand into a free zone [11,12]. The cells became mobilized progressively inward, and mechanical quantities such as tension exhibit a wave-like pattern on the kymographs [12]. To our knowledge, there has been so far no consensus on the exact nature of these waves. In our interpretation, the early-time waves that initiate from both boundaries, travel inward, and cross each other, are related to the sudden release of the confining barrier. The later-time waves in those experiments might be echos of early-time waves, but might also be associated with increased cell division.

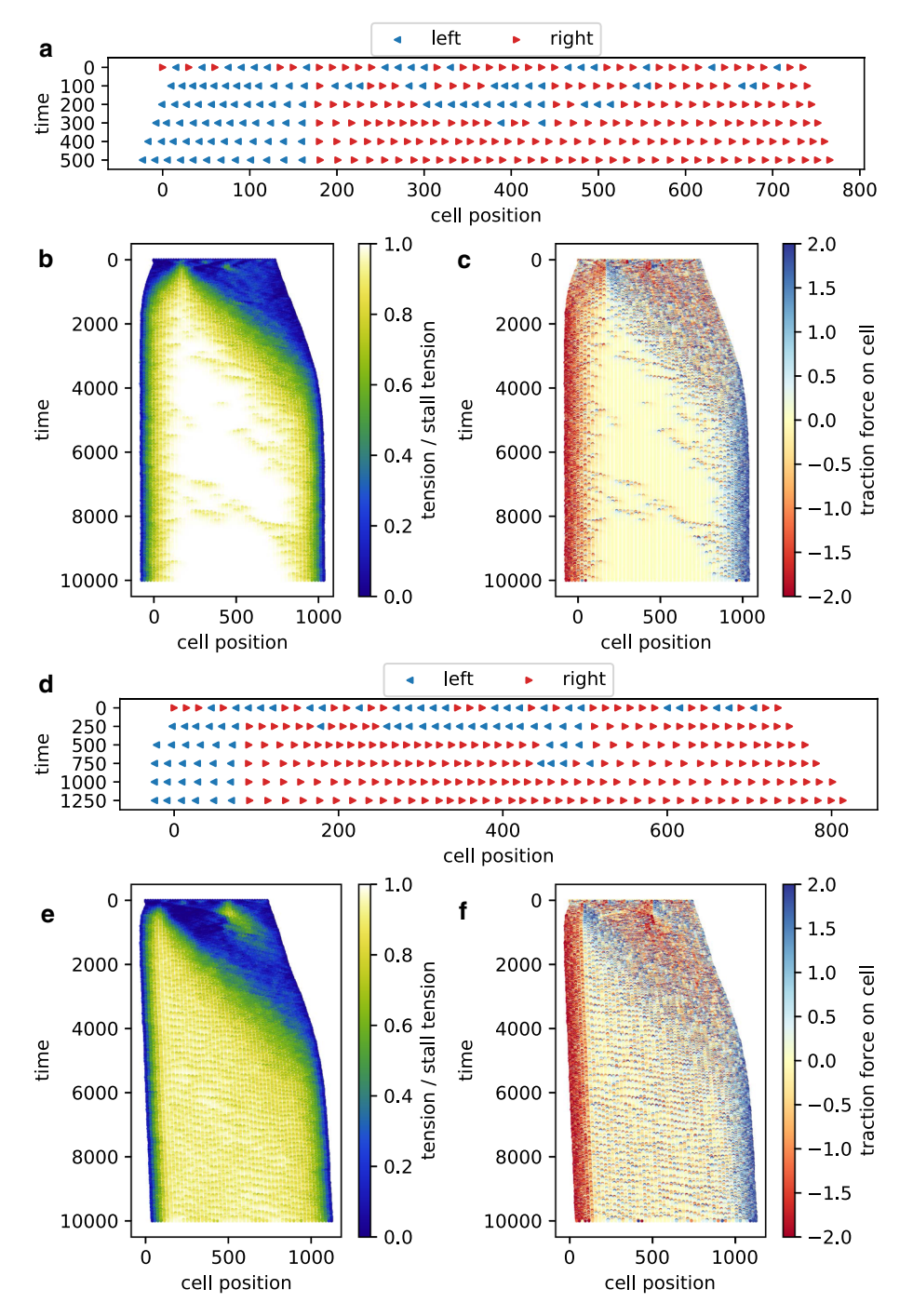
In experiments, there are symmetrically and asymmetrically expanding clusters [12], as in our simulations with initial random polarity leading to different domain sizes. We will focus on a symmetric case with two equal domains, with 25 cells on left and right with left/right polarity, respectively (Fig. 4a). Due to our CIL rules, there is no polarity reversal in these simulations (Fig. 4a).

It is not surprising that there is a finite time delay before the influence of barrier removal reaches the inner cells. In general, one should expect a finite relay speed of mechanical response in cell colonies. Such a delay would appear as a "V" or "X" pattern on a kymograph, with arms initiating from boundaries and meet at the middle. We hypothesize that the prolonged initial confined growth induces compression of the cells, the release of which then leads to the crossed waves. To show this, we placed harmonic potentials acting as walls on both sides and changed the rest length of inter-cellular springs such that all the cells are under compression that is large enough so cells basically are stopped (recall Eq. 6). At the 2000-th step, the two walls are removed. As shown in Fig. 4b, because of the mechanism in Eq. 6, cell mobilization progresses gradually inward, and the tension accumulates, beginning from center then proceeding outward. In Fig. 4c, it is shown that the blue and red colors exchange position once they meet at the center at around the 3000-th step, so there is crossing rather than bouncing-back or reflection. That is, our simulation supports the "X"wave observed in experiments [12].

This accounts for the waves immediately after release [12]. For later times, if in the experiment the further wave is actually echos, i.e., reflection of the initial waves



Fig. 3 (a-c) Polarity at selected times and kymographs of tension and traction for a static cluster consisting of two unequal-sized domains. (d-f) Same quantities for a moving cluster where the left domain has too few cells to stall the interior



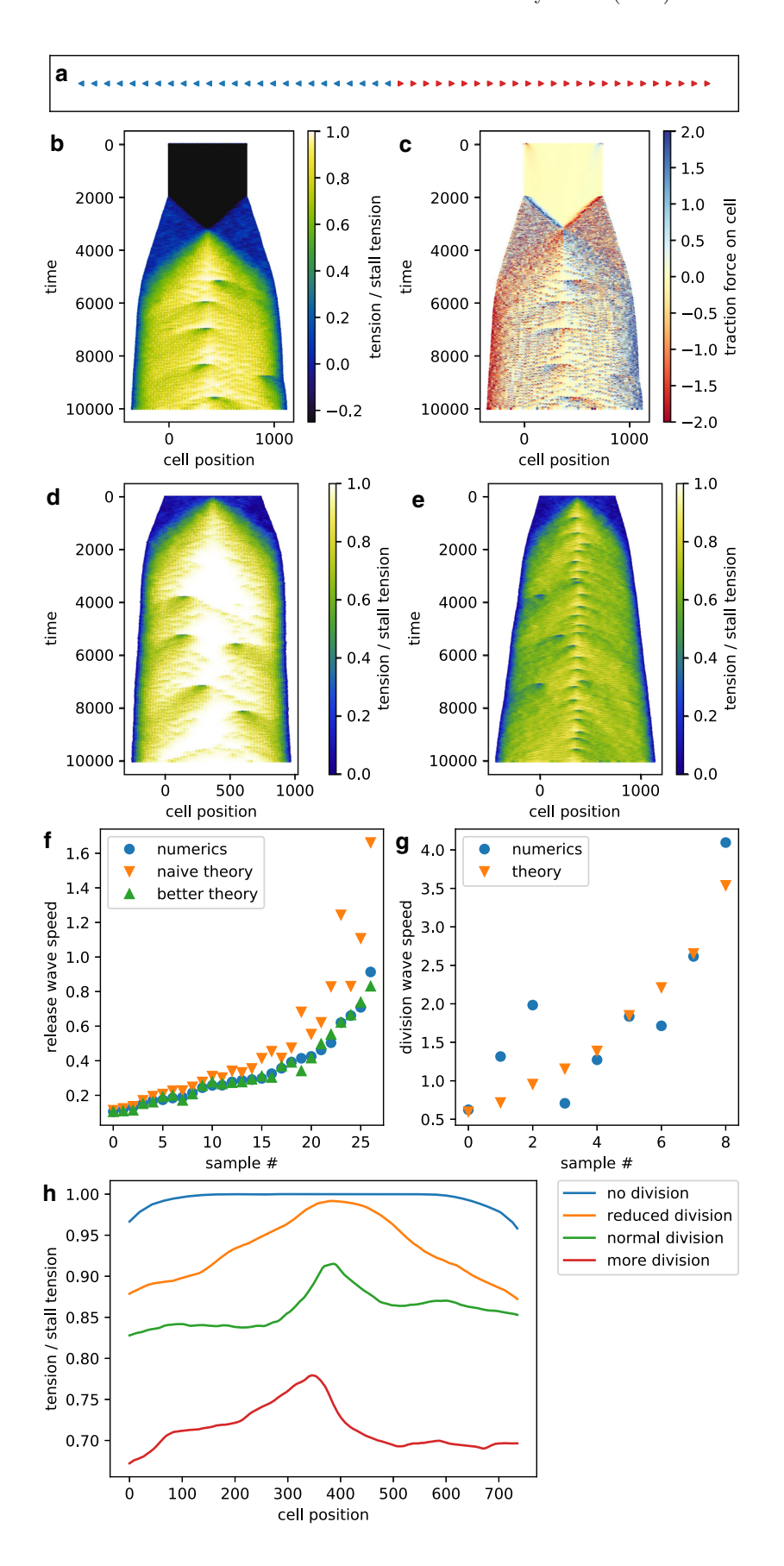
off the colony boundary, this may indicate a longer time influence of the original confinement than is present in our treatment. Our model does not show these echos they dissipate after reaching the opposite boundary. What we show instead is that cell division is a possible source for later-time waves.

With cell proliferation, the clusters grow indefinitely as long as the critical division tension $T_{\rm div}$ is smaller than T_s . Interestingly, there is now a new source of wave-like excitation, launched from cell division sites (Fig. 4b, c). Specifically, whenever a new cell is born, there is a strong local density perturbation and this appears to launch a density wave in the cluster which then propagates to the boundary. We understand the waves as arising simply because there is a time delay for a cell to start to move from its stalled state to accommodate the presence of the new cell. These waves are better separated when division is infrequent (Fig. 4d), and are more overlapped when division is more frequent (Fig. 4e). In Fig. 4d, it is clear that each wave arm consists of an upper edge where cells sequentially un-stall, and a lower edge where cells restore stalling.

In 2D expansion experiments, the rectangular colony spans a much larger length in y-direction, and the kymographs are constructed by taking average or median values across y-direction and focused on expan-



Fig. 4 Waves in cell clusters due to confinement release and due to proliferation. (Caption continued on a different page.) Waves in cell clusters due to confinement release and due to proliferation. a Initial setup of the cluster. b, c Cell midpoint tension, traction kymographs of a proliferating cluster with pre-confinement, where l_0 is increased to 10 from that in Table 1. See also SI Fig. 10 d, e Cell midpoint tension kymographs for a d less / e more frequently proliferating cluster. See also SI Figs. 11, 12, and 13. f Release wave speed measurements and estimations. Twenty-seven samples were generated with varied v_f , F_{hs} , l_0 . g Division wave speed measurements and estimations. Nine samples were generated with varied v_f and initial separation between adjacent cell midpoints $\Delta x_c^{(init)}$. For the exact parameter variations in f, g see SI Sect. 5. h Cell midpoint tension averaged over the latter half of a trajectory for different division frequencies. The exact division-related parameter variations can be found under SI Fig. 4





sion in x-direction. Therefore, the division events across a long line parallel to y-axis are unlikely to be synchronized. How this asynchrony would affect the divisionwave pattern on such a kymograph awaits elucidation by extensions of our current model to the twodimensional case.

Proliferation events also change the tension distribution across the cluster. As shown in Fig. 4h, the tension has a clear plateau shape in the absence of division. As division becomes more frequent, the average interior tension decreases and the peak at the center is sharper. Then, due to the peaked distribution, cell division events are more likely near the center. Although such a division would cause stress relief, the rapid propagation away from the initiation point of the waves quickly restores the center region to being the most tensile. This behavior could account for the observation of [10] where the tension gradient is not confined to the surface layers; we note that the experimental data comes from a 2D system and represents an average over some distance in the longitudinal direction, and this may smooth out the structure as compared to our 1D simulation results. These division events are also a source of noise in the interior. Since the interior is now not completely stalled, there is fluctuating, nonzero traction with the substrate from inner cells (Fig. 4c), as compared to Fig. 2.

It is worthwhile to compare these two different wave phenomena seen in our model. We relate the early-time wave pattern to the response to pre-confinement, and late-time to accommodation to cell divisions. Both are attributable to the inherent finite response to perturbations which alter the cell's motility from a state in which that motility was suppressed. The former type of wave initiates from the boundaries and propagates inward, while the latter initiates at the center and propagates outward. To demonstrate the underlying physics, we can look at the propagation speeds for both wave types. For the release wave, the wave speed measures how fast successive cells are "activated" one by one. Label the cells from outside as 0-th, 1-st, and so on, and consider the time needed between the sequential activation of ith and (i + 1)-th cell. The distance the wave travels is the initial separation between adjacent cell midpoints $\Delta x_c^{(init)}$. We approximate the *i*-th cell as traveling at the speed of single free cell speed v_1 , which can be easily calculated from a single cell simulation. It needs to travel for a distance of $l_0 - (\Delta x_c^{(init)} - 2L_0) - F_{hs}/k$ (See Table 1 for parameter definitions) before the compression on the next cell's front is less than F_{hs} allowing the next one to be activated. This gives a "naive theory" of wave speed

$$\frac{\Delta x_c^{(init)} v_1}{l_0 - (\Delta x_c^{(init)} - 2L_0) - F_{hs}/k}$$

(see Fig. 4f). An improvement is made by considering that each cell except for the 0-th one linearly accelerates from zero to v_1 . When the (i-1)-th cell's displacement is between $l_0 - (\Delta x_c^{(init)} - 2L_0) - F_{hs}/k$ and $l_0 - (\Delta x_c^{(init)} - 2L_0)$, the (i-1)-th travels at v_1 , but the *i*-th cell travels at mean speed of $v_1/2$ because of the linear acceleration. That is, the *i*-th cell travels at mean speed $v_1/2$ for a duration of $F_{hs}/(kv_1)$, then travels at v_1 for the rest distance of $l_0 - (\Delta x_c^{(init)} - 2L_0) - F_{hs}/k - (v_1/2)(F_{hs}/(kv_1))$, before calling up the (i+1)-th cell. This gives a "better theory" of wave speed

$$\frac{\Delta x_c^{(init)} v_1}{l_0 - (\Delta x_c^{(init)} - 2L_0) - F_{hs}/(2k)}$$

(see Fig. 4f). For the division-launched wave, note that the influence of insertion of the new-born cell is transmitted most strongly when the nearest cell to the division site protrudes, so one can estimate the wave upper edge (sequential un-stalling) speed to be $(l_0 + T_s/k +$ $(2L_0)/T_{cycle}$, namely the distance between midpoints of adjacent stalled cells divided by time length of a contraction cycle. Note that T_{cycle} is inversely proportional to v_1 and can be similarly calculated from a single-cell simulation. Given the diffuse nature of these division waves, the measurement can be hardly accurate, but this theory still approximately agrees with numerics (Fig. 4g). In principle, one can use these relations to distinguish different wave types in real experiments.

The waves observed in [14] seem to be different from what we have discussed so far. The authors interpret their wave observations as arising from a spontaneous instability in their system which gives rise to repeated wave launches, presumably arising from the amplification of fluctuations. We have not observed such an instability in our simulations. We believe that the instability of [14] arises from a process that we do not have in our model. We can see this by examining their continuum theory. The process that gives unstable behavior is that the mean propulsive force of cells increases with strain. The underlying process seems to be that in a two-dimensional layer, uniaxial strain will align cells. Then, a velocity fluctuation will cause additional strain which aligns more cells, giving positive feedback. Of course, our one-dimensional simulation cannot support such a process. In our model cell contraction and protrusion play the role of propulsive force, and in the molecular clutch scheme (Eq. 1), contraction slows down as strain increases. For a real system, it is plausible that both effects might occur. Which one dominates probably depends on parameters and cell density. We should note that in [10,12] there is no sign of an instability.

3.3 Periodic boundary conditions

In the experiment of [15], cells move along a 1D annulus. Initially, clusters expand but once the ends contact each other around the annulus, there is a transition between a state with expansion with proliferation and one with collective motility (rotation) without cell division. To treat this case, we simulated a cluster growing



in a 1D periodic domain, ignoring any possible effect due to ring curvature. An extra inter-cellular spring between the two outermost cells in our colony is added when the cluster has expanded enough to "fill the annulus." Specifically for this simulation, this size occurs at the 5000-th step and thereafter the left- and right-most cells are joined by an adhesion; see Fig. 5. Note that in these simulations we have enhanced the rate of cell division by taking $F_{div} = 0.9 \ T_s$ (instead of 0.99 T_s) to speed up cluster growth. As can be seen, our simulation directly captures the observed transition.

The mechanism underlying the transition is that when the two outer ends of the cluster collide as the cells fill the annulus (i.e., when the new spring is attached), the CIL process becomes active. To capture the transition details, we plotted the polarity and cell length in a kymograph (Fig. 5a). In our simulations, the cluster always chooses one or the other polarity, and starts to revolve around the annulus. The resulting colony remains weakly tensile (Fig. 5b, d). Recalling that the condition for CIL re-polarization requires collision; individual cell(s) may not immediately orient so as to agree with the majority polarity, but are nonetheless dragged along (See the red segment after the 5000-th step in Fig. 5a). The reversal of polarity takes place in a wave (the sloping border between red and blue in Fig. 5a and the corresponding "scar" in b-d). The nature of this wave is similar to that of the density waves discussed above, involving finite delay in response to mechanical perturbations. There is a characteristic time for reversal of polarity, the inverse of the rate in Eq. 7. The speed of the reversal wave is of the order of the cell separation divided by this time. Finally, the transition to rotation may not be so smooth. In some cases, the domain border is zigzag shaped on the kymograph. See SI Figs. 14, 15, and 16 for examples.

4 Summary and conclusions

We have introduced a one-dimensional mechanical model for cells that are attached to each other and to a substrate and move collectively. The cells undergo a contraction-protrusion cycle. To account for the fact that contraction is based on myosin mini-filaments walking along actin fibers, we have used a molecular clutch formulation of the connection between the stress state of the cell and the contractile velocity. Adhesion is represented by springs connecting points along the cell to a rigid substrate.

These adhesive springs come and go and cell polarity determines which half of the cell has a higher number of such adhesions. We have also incorporated a simplified form of the well-established biological mechanism CIL, contact inhibition of locomotion. This form of CIL consists of slowing down the cell when it encounters an obstacle and also reversing the polarity by moving adhesive sites of two cells engaged in a head-on collision.

Given its relative simplicity, it is remarkable how many interesting aspects of collective cell motility this model is able to demonstrate, including a resolution of an apparent conflict between plateau and peak stress patterns observed in different experiments, and an explanation for the waves.

The eventual mechanical state of a cell cluster can be of one of several types. In the absence of any cell division, the cluster size eventually must saturate. If the cluster is relatively symmetric, that is there are a significant number of cells in the right-polarized domain engaging in a tug-of-war of with a significant number of left-polarized cells, the cluster will stop moving altogether and the inter-cellular tension will exhibit a broad plateau. This is similar to the mechanical state observed in [11,12]. In those experiments there is proliferation, but this model picture barely changes when proliferation is infrequent. The plateau region is composed of a large number of cells that have stalled and hence are no longer actively contracting. The tension at the plateau then falls to zero over a finite-size transition region at the two edges. Interestingly, there is no translation of the cluster even if the number of differently polarized cells are unequal; this is because the number of actively pulling cells is the same on both sides and the different numbers of stalled cells make no difference. A different possibility is the polarity pattern with only a small number of cells in the thinner polarity domain, smaller than the transition region width. The limiting case here is when all the cells are polarized in the same direction. Then, the cells are never stalled, and the entire cluster moves systematically.

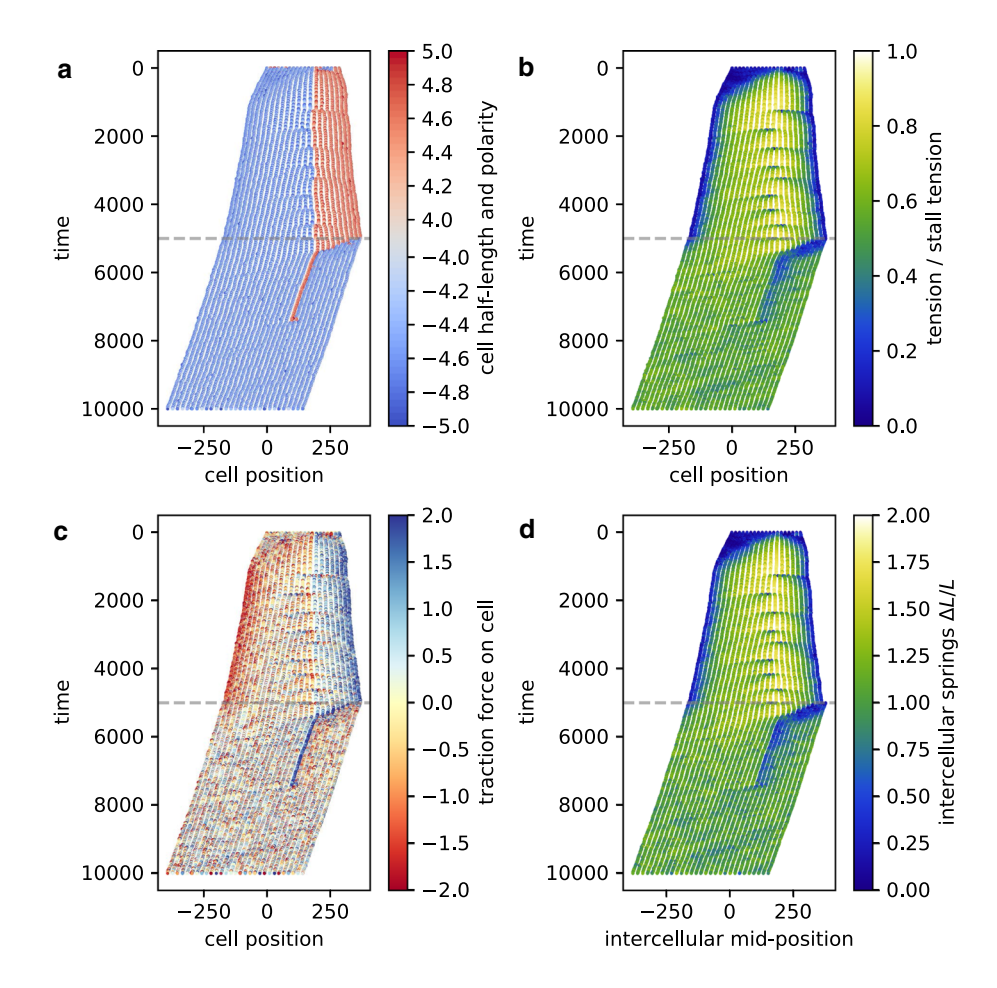
When there is cell division the cluster can grow indefinitely. It is thought that cell division is directly coupled to the size of cells [36–38] which in our model is directly determined by the tensile stress. In our model, we have therefore allowed a cell to divide if its tension gets close to the stall value. For small rates of cell division, the previous "plateau" state is relatively unchanged except for the fact that it continues to slowly expand, simply by adding more stalled cells to the cluster interior.

Our model can explain the occurrence of waves emerging from the cluster boundary once it is released from confinement and allowed to expand. In our model, these results come simply from the time it takes for a cell to recover motility when it ceases being stopped by a barrier. In our model cell division events also each lead to a propagating disturbance, moving faster than the expansion rate and hence hitting the cluster boundary and dissipating. Again, the propagating disturbance is simply due to the transient un-stalling resulted from the local tension release created by the newborn cell. As argued above in a two-dimensional system these disturbances may be asynchronous, thus complicate the projected kymograph. However, they at least have the observable effect that they can give rise to traction noise within the cluster as in [12].

As the disturbances relax the stall condition, cells in the interior undergo active contraction and hence contribute to the net traction force. This tends to destroy the plateau and spreads the tension gradient region over the entire cluster. This type of pattern is similar to what was observed in [10], where the tension gradient exists



Fig. 5 Space-time plot of a simulated cell cluster on a ring. It keeps expanding until two outermost cells are joined by a spring at t= 5000, indicated by the grav dashed line. a Polarity and half-length of the cells. Blue or negative sign denotes "left" polarity and red/positive denotes "right." **b** Cell midpoint tension, c Traction force on each cell by substrate due to the adhesions. d Inter-cellular tension stress, i.e., the stretch of the inter-cellular springs. Note that the rightmost new spring created at t = 5000 is the one connecting two outermost cells



over several millimeters worth of tissue. An alternative explanation for this behavior is in [18], but it did not illustrate the possible transition between a plateau and a peak.

We have also illustrated the experiment in [15] where cells were constrained to move along an annulus. As an initially small cluster expands, the two ends eventually collide and the cluster transitions to the coherent motion state with almost all the cells having the same polarity and no division taking place. We observe that this transition takes place by a polarity reversing wave that eventually leads to a large preponderance of cells moving the same way. Again, wave-like phenomena have been seen in colliding tissues [41]. There can be individual "rebellious cells" that maintain the "wrong" polarity, but these have little effect on the overall cluster behavior.

In our work, we have assumed a completely rigid substrate. In fact, experiments are usually performed on compliant substrates which allows tractions to be measured. However, we do not expect this to make a qualitative difference in the results given here since the loading of the intra- and inter-cellular strain into the substrate is probably small for the conditions of the experiments. Often cells move quite differently (or not at all) on very compliant substrates; [42], but this is not the case at hand. If we introduce substrate compliance in future work, we would be able to treat collective durotaxis, which has been observed for these clusters

It should be straightforward conceptually to extend to a two-dimensional model that includes similar contraction-protrusion dynamics. This extension has already been accomplished for single-cell motility, with the major changes being that now both force and torque need to be balanced at each step of the simulation, and the fact that polarity now becomes a vector which determines the direction of the protrusion [34]. The practical challenge for collective motility is to have reasonable and tractable inter-cell adhesions when cells can each move in any direction.

Cells are extremely complex mechanical objects and of course one cannot expect to describe all their phenomenology with simple models. However, at least for collective behavior we may expect (or at least hope) that many of the biological details are not critical when it comes to grasping the essence of what can occur. The results reported here should give us added confidence in this physics-based approach.

Supplementary information The online version contains supplementary material available at https://doi.org/ 10.1140/epje/s10189-021-00141-7.



Acknowledgements This work was supported in part by the National Science Foundation Center for Theoretical Biological Physics NSF PHY-2019745, and also by PHY-1605817 and NSF-EFRI-1741618.

Author contribution statement

All authors designed and conducted the research, analyzed the data, and wrote the manuscript.

References

- D.P. Thomas, G.G. Borisy, Cellular motility driven by assembly and disassembly of actin filaments. Cell 112(4), 453–465 (2003)
- P. Friedl, J. Locker, E. Sahai, J.E. Segall, Classifying collective cancer cell invasion. Nat. Cell Biol. 14(8), 777–783 (2012)
- Vincent Hakim, Pascal Silberzan, Collective cell migration: a physics perspective. Rep. Progress Phys. 80(7), 076601–47 (2017)
- C.G. Kleer, K.L. van Golen, T. Braun, S.D. Merajver, Persistent E-Cadherin expression in inflammatory breast cancer. Modern Pathol. 14(5), 458–464 (2001)
- M.K. Jolly, M. Boareto, B.G. Debeb, N. Aceto, M.C. Farach-Carson, W.A. Woodward, H. Levine, Inflammatory breast cancer: a model for investigating clusterbased dissemination. NPJ Breast Cancer 3(1), 1–8 (2017)
- M.C. Marchetti, J.-F. Joanny, S. Ramaswamy, T.B. Liverpool, J. Prost, M. Rao, R.A. Simha, Hydrodynamics of soft active matter. Rev. Modern Phys. 85(3), 1143 (2013)
- A.S. Yap, W.M. Brieher, B.M. Gumbiner, Molecular and functional analysis of cadherin-based adherens junctions. Ann. Rev. Cell Dev. Biol. 13(1), 119–146 (1997)
- 8. Roberto Mayor, Carlos Carmona-Fontaine, Keeping in touch with contact inhibition of locomotion. Trends Cell Biol. **20**(6), 319–328 (2010)
- Xavier Trepat, Erik Sahai, Mesoscale physical principles of collective cell organization. Nat. Phys. 14(7), 671–682 (2018)
- X. Trepat, M.R. Wasserman, T.E. Angelini, E. Millet, D.A. Weitz, J.P. Butler, J.J. Fredberg, Physical forces during collective cell migration. Nat. Phys. 5(6), 426– 430 (2009)
- R. Sunyer, V. Conte, J. Escribano, A. Elosegui-Artola, A. Labernadie, L. Valon, D. Navajas, J.M. García-Aznar, J.J. Muñoz, P. Roca-Cusachs, X. Trepat. Collective cell durotaxis emerges from long-range intercellular force transmission. Science (New York, NY), 353(6304):1157–1161, September 2016
- X. Serra-Picamal, V. Conte, R. Vincent, E. Anon, D.T. Tambe, E. Bazellieres, J.P. Butler, J.J. Fredberg, X. Trepat, Mechanical waves during tissue expansion. Nat. Phys. 8(8), 628–634 (2012)
- C. Pérez-González, R. Alert, C. Blanch-Mercader, M. Gómez-González, T. Kolodziej, E. Bazellieres, J.

- Casademunt, X. Trepat, Active wetting of epithelial tissues. Nat. Phys. 8(2), 026014 (2019)
- Sham Tlili, Estelle Gauquelin, Brigitte Li, Olivier Cardoso, Benoît Ladoux, Hélène. Delanoë-Ayari, François Graner, Collective cell migration without proliferation: density determines cell velocity and wave velocity. R. Soc. Open Sci. 5(5), 20–172421 (2018)
- S. Jain, V.M.L. Cachoux, G.H.N.S. Narayana, S. de Beco, J. D'Alessandro, V. Cellerin, T. Chen, M.L. Heuzé, P. Marcq, R.-M. Mège, A.J Kabla, C.T. Lim, B. Ladoux, The role of single-cell mechanical behaviour and polarity in driving collective cell migration. Nat. Phys., 10:1–8 (2020)
- C. Blanch-Mercader, R. Vincent, E. Bazellières, X. Serra-Picamal, X. Trepat, J. Casademunt, Effective viscosity and dynamics of spreading epithelia: a solvable model. Soft Matter 13(6), 1235–1243 (2017)
- S. Banerjee, K.J.C. Utuje, M. Cristina Marchetti, Propagating stress waves during epithelial expansion. Phys. Rev. Lett. 114(22), 228101–228105 (2015)
- J. Zimmermann, B.A. Camley, W.-J. Rappel, H. Levine, Contact inhibition of locomotion determines cell-cell and cell-substrate forces in tissues. Proc. Natl. Acad. Sci. U S A 113(10), 2660–2665 (2016)
- J.J. Williamson, G. Salbreux, Stability and roughness of interfaces in mechanically regulated tissues. Phys. Rev. Lett. 121(23), 238102 (2018)
- Ricard Alert, Carles Blanch-Mercader, Jaume Casademunt, Active fingering instability in tissue spreading. Phys. Rev. Lett. 122(8), 088104 (2019)
- Y. Yang, H. Levine, Leader-cell-driven epithelial sheet fingering. Phys. Biol. 17, 046003 (2020)
- F. Graner, J.A. Glazier, Simulation of biological cell sorting using a two-dimensional extended Potts model. Phys. Rev. Lett. 69(13), 2013 (1992)
- Reza Farhadifar, Jens-Christian. Röper, Benoit Aigouy, Suzanne Eaton, Frank Jülicher, The influence of cell mechanics, cell-cell interactions, and proliferation on epithelial packing. Curr. Biol. 17(24), 2095–2104 (2007)
- B.A. Camley, Y. Zhang, Y. Zhao, B. Li, E. Ben-Jacob, H. Levine, W.-J. Rappel, Polarity mechanisms such as contact inhibition of locomotion regulate persistent rotational motion of mammalian cells on micropatterns. Proc. Natl. Acad. Sci. 111(41), 14770–14775 (2014)
- 25. Sara Najem, Martin Grant, Phase-field model for collective cell migration. Phys. Rev. E $\bf 93(5),~052405~(2016)$
- Tamás Vicsek, András Czirók, Eshel Ben-Jacob, Inon Cohen, Ofer Shochet, Novel type of phase transition in a system of self-driven particles. Phys. Rev. Lett. 75(6), 1226 (1995)
- Markus Basan, Jens Elgeti, Edouard Hannezo, Wouter-Jan. Rappel, Herbert Levine, Alignment of cellular motility forces with tissue flow as a mechanism for efficient wound healing. Proc. Natl. Acad. Sci. 110(7), 2452–2459 (2013)
- 28. C.E. Chan, D.J. Odde, Traction dynamics of filopodia on compliant substrates. Sci. (N. Y. NY) **322**(5908), 1687–1691 (2008)
- B.L. Bangasser, G.A. Shamsan, C.E. Chan, K.N. Opoku, E.T. Uuml Zel, B.W. Schlichtmann, J.A. Kasim, B.J. Fuller, B.R. McCullough, S.S. Rosenfeld, D.J. Odde, Shifting the optimal stiffness for cell migration. Nat. Commun. 8, 1–10 (2017)



- 30. J. Escribano, R. Sunyer, M.T. Sánchez, X. Trepat, P. Roca-Cusachs, J.M. García-Aznar, A hybrid computational model for collective cell durotaxis. Biomech. Model. Mechanobiol. 17(4):1037-1052 (2018)
- 31. N. Yamana, Y. Arakawa, T. Nishino, K. Kurokawa, M. Tanji, R.E. Itoh, J.M., Toshimasa Ishizaki, H. Bito, K. Nozaki, et al., The rho-mdia1 pathway regulates cell polarity and focal adhesion turnover in migrating cells through mobilizing apc and c-src. Mol. Cell. Biol., 26(18):6844-6858 (2006)
- 32. Alex Mogilner, Mathematics of cell motility: have we got its number? J. Math. Biol. **58**(1–2), 105–134 (2009)
- 33. M. Buenemann, H. Levine, W.-J. Rappel, L.M. Sander, The role of cell contraction and adhesion in dictyostelium motility. Biophys. J., 99(1):50-58 (2010)
- 34. J. Feng, H. Levine, X. Mao, L.M. Sander, Cell motility, contact guidance, and durotaxis. Soft Matter 15, 4856-
- 35. Yanjun Yang, Herbert Levine, Role of the supracellular actomyosin cable during epithelial wound healing. Soft Matter 14(23), 4866-4873 (2018)
- A. William, Wells, does size matter? J. Cell Biol. 158(7), 1156-1159 (2002)
- 37. Markus Basan, Jacques Prost, Jean-François. Joanny, Jens Elgeti, Dissipative particle dynamics simulations for biological tissues: rheology and competition. Phys. Biol. 8(2), 026014 (2011)

- 38. S.J. Streichan, C.R. Hoerner, T. Schneidt, D. Holzer, L. Hufnagel, Spatial constraints control cell proliferation in tissues. Proc. Natl. Acad. Sci. 111(15), 5586-5591
- 39. Dhruv K. Vig, Alex E. Hamby, Charles W. Wolgemuth, Cellular contraction can drive rapid epithelial flows. Biophys. J. 113(7), 1613-1622 (2017)
- 40. Somanna A. Kollimada, Ankur H. Kulkarni, Aniket Ravan, Namrata Gundiah, Advancing edge speeds of epithelial monolayers depend on their initial confining geometry. PLoS ONE 11(4), e0153471 (2016)
- 41. P. Rodríguez-Franco, A. Brugués, A. Marín-Llauradó, V. Conte, G. Solanas, E. Batlle, J.J. Fredberg, P. Roca-Cusachs, R. Sunver, X. Trepat, Long-lived force patterns and deformation waves at repulsive epithelial boundaries. Nat. Mater., 16(10):1029-1037 (2017)
- 42. T.A. Ulrich, E.M. de Juan Pardo, S. Kumar, The mechanical rigidity of the extracellular matrix regulates the structure, motility, and proliferation of glioma cells. Cancer Res., 69(10):4167-4174 (2009)

